# Study of melting and freezing in the Gaussian core model by molecular dynamics simulation

Frank H. Stillinger and Thomas A. Weber

*Bell Laboratories, Murray Hill, New Jersey 07974*
(Received 11 October 1977)

Molecular dynamics calculations have been carried out to establish quantitative properties of the Gaussian core model near its crystal–fluid transition. Two densities have been considered, for both of which the stable crystal structure at absolute zero is body-centered cubic. Spontaneous melting and freezing events were observed at both densities. Annealing of defective crystalline phases and formation of amorphous "glassy" structures have been induced. Properties for the model at equilibrium display some surprising "waterlike" anomalies, including negative volume of melting, negative thermal expansion in the fluid, and increase in rate of self-diffusion as the system is compressed.

## I. INTRODUCTION

It has been pointed out recently[1] that the "Gaussian core model" offers a convenient and illuminating way to study phase transitions, in particular to study the fluid–solid transition. This model consists of structureless point particles which move according to the laws of classical mechanics, and which interact in pairs with a repelling Gaussian potential:

$$\phi(r_{ij}) = \phi_0 \exp[-(r_{ij}/l)^2], \qquad \phi_0, l > 0. \tag{1.1}$$

The total potential energy $\Phi$ for a collection of $N$ Gaussian core particles is then taken to be

$$\Phi(\mathbf{r}_1 \cdots \mathbf{r}_N) = \sum_{i<j=1}^{N} \phi(r_{ij}). \tag{1.2}$$

It has been suggested[1] that some polymer solutions may behave osmotically as though $\Phi$ were the potential of mean force acting between macromolecular centroids.

The Gaussian core model is known to possess several interesting properties. Among these are the following[1]:

(a) Distinct temperature–density regions in which the body-centered-cubic and face-centered-cubic crystal structures, respectively, are thermodynamically stable;

(b) A compression-melting phenomenon which leads to a density of maximum melting temperature, and hence to regions of both positive and negative volumes of melting;

(c) Reduction to hard-sphere-model behavior in a suitable low-temperature, low-density limit.

The Gaussian core model also possesses an important mathematical advantage. Its classical partition function can be expanded in an asymptotic inverse-temperature series, with coefficients that can be evaluated explicitly. Any classical model (with bounded $\Phi$) can formally be expanded in such a series, where the coefficients consist of irreducible cluster integrals that are generated by the cumulants (semi-invariants) of $\Phi$.[2] The present model has the unique attraction that its cluster integrals reduce to elementary integrals by diagonalizing symmetric quadratic forms. Indeed, it was this singular feature which caused the Gaussian core model to be considered in the first place.

In preparation for a detailed study of the inverse-temperature series, it was deemed essential to determine quantitatively accurate properties for the Gaussian core model by an independent means. For this purpose we have turned to computer simulation. The present paper reports some results obtained by the "molecular dynamics" approach.[3] We have examined both solid and fluid phases, as well as transformations between them.

An unexpected finding in this simulation study was that the Gaussian core model in some respects is "waterlike." One such attribute is the negative melting volume already mentioned. Others are negative thermal expansion in the fluid phase,[4] and increase in self-diffusion rate upon isothermal compression.[5] Since interactions in the present model differ drastically from those in water, credible explanation of the eccentric behavior of water[6] must henceforth be tempered by the knowledge that the eccentricity can arise in a variety of ways.

We discuss technical details of our molecular dynamics approach in Sec. II. This is followed by an exposition of simulation results obtained thus far concerning thermodynamic behavior (Sec. III), local structure (Sec. IV), diffusion rates (Sec. V), and dynamics of phase transformation (Sec. VI).

## II. MOLECULAR DYNAMICS METHOD

We rely upon a digital computer to provide numerical solutions to the $3N$ coupled Newton equations of motion for the $N$ particles with mass $m$:

$$m d^2\mathbf{r}_j/dt^2 = -\nabla_j \Phi \qquad (j = 1 \cdots N). \tag{2.1}$$

These differential equations must of course be supplemented by initial conditions on positions and momenta. The integration procedure and subsequent analysis can be carried out most conveniently in terms of reduced units that are natural for the model: $\phi_0$, $l$, and $(ml^2/\phi_0)^{1/2}$ were adopted as units of energy, length, and time, respectively.

We initially carried out a series of preliminary calculations in the fluid phase using systems of 500 particles. However, the bulk of our subsequent calculations have utilized 432 particles. Only very minor quantitative differences were perceptible in comparing

 0021-9606/78/6808-3837$01.00  

these two system sizes. We believe that the infinite-system limiting behavior can be accurately inferred from calculations with 432 particles, provided that certain precautions mentioned below are duly observed.

In all cases the $N$ particles were confined to a cubical cell with volume $V$ chosen to yield the density of interest. Periodic boundary conditions have consistently been employed. As usual, the system energy (and thus the temperature) can be manipulated by scaling momenta.

The calculations reported here involve only two values of the dimensionless density $\rho^* = Nl^3/V$, namely, 0.4 and 1.0. Prior work[1] has revealed that the body-centered-cubic crystal is apparently the stable low-temperature structure for both of these densities. The reason for using 432 particles is simply that this number can form a perfect body-centered-cubic crystal with the given cubical cell and periodic boundary conditions. Another value of $N$ (not equal to twice a perfect cube) would either lead to a metastable crystal structure or to a necessarily defective body-centered-cubic crystal at absolute zero of temperature.

A fifth-order algorithm due to Gear[7] has been used to integrate differential equations (2.1) after expressing them in reduced units. Time increment $\Delta t^*$ for integration was set equal to 0.05 (in reduced units), which had the effect of holding drifts in total energy and center-of-mass momentum (nominally conserved quantities) within acceptably narrow limits. The number of time steps required to investigate a given thermodynamic state was variable, but usually a period of 2000 $\Delta t^*$ was first allowed to elapse to achieve equilibration, and a period of 2000 $\Delta t^*$ to 10000 $\Delta t^*$ was subsequently utilized to form averages. Except within the phase transition region, the results were stable and reproducible. Over 70 distinct thermodynamic states at the two densities have been examined.

For the purpose of initiating a series of runs we have used both random initial positions, as well as a perfect body-centered-cubic array. The former is useful in mapping out the behavior of the fluid phase

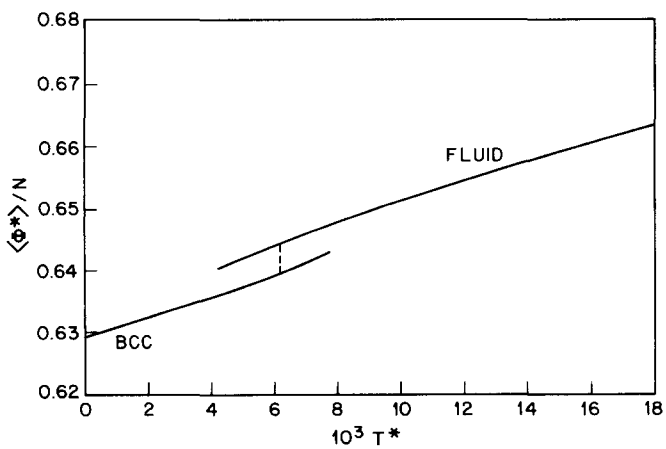


FIG. 1. Potential energy per particle at reduced density 0.4. The dotted line locates the thermodynamic transition.

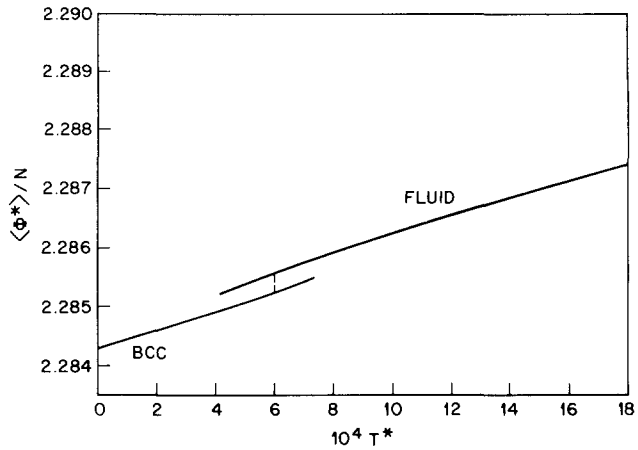


FIG. 2. Potential energy per particle at reduced density 1.0.

by successive stages of cooling. The latter provides analogous information for the solid. However, we also observe phase transitions to the opposite phase as discussed below, to check on reproducibility.

## III. THERMODYNAMIC FUNCTIONS

Figures 1 and 2 present values computed for the average reduced potential per particle $\langle\Phi\rangle/N\phi_0$ (denoted for simplicity as $\langle\Phi^*\rangle/N$), at densities 0.4 and 1.0, respectively. In both cases separate and disconnected branches were obtained for the low-temperature crystal and the high-temperature fluid. The phase transitions between these states are first order, with change in fundamental phase symmetry.

It is characteristic of the molecular dynamics simulation that metastable extensions of crystal and fluid branches are inevitable beyond the thermodynamic transition point. This stems from the sluggishness with which spontaneous nucleation of the new phase occurs in the absence of a suitable "seed" or container-supplied epitaxial growth site. But in spite of this metastability, it is possible to locate the transition points reasonably accurately by the means discussed below in Sec. VI.

For an infinite system undergoing a first-order phase change, subject to a constant volume constraint, a finite temperature interval of phase coexistence should in principal exist. In the present case this implies that the temperature $T_m$ at which a warming crystal begins to melt reversibly is less than the temperature $T_f$ at which a cooling fluid begins to freeze reversibly. However, $T_m$ and $T_f$ are not distinguishable in the calculations we have performed, partly because of finite system size effects, partly because of incomplete phase space averaging, and partly because these temperatures probably differ by less than a percent under our prevailing conditions.

We have concluded from our extensive studies that the transitions thermodynamically occur at the following reduced temperatures:

$$T_m^* \cong T_f^* = 6.2 \pm 0.3 \times 10^{-3} \quad (\rho^* = 0.4) \qquad (3.1)$$
$$= 6.0 \pm 0.5 \times 10^{-4} \quad (\rho^* = 1.0)\,,$$

where we use

$$T^* = k_B T/\phi_0 \,. \tag{3.2}$$

The dramatic decline in transition temperature as the density increases clearly illustrates the compression melting phenomenon identified earlier for the model.[1]

The changes in potential energy per particle occurring at the transition were found to be

$$\begin{aligned}\langle \Delta\Phi^* \rangle/N &= 5.02 \pm 0.05 \times 10^{-3} \quad (\rho^* = 0.4) \\ &= 3.24 \pm 0.20 \times 10^{-4} \quad (\rho^* = 1.0) \,.\end{aligned} \tag{3.3}$$

Except for an insignificant correction (to account for the constant-density restraint), these are the transition enthalpies.

The corresponding entropies of transition may be obtained by dividing the results (3.3) by the corresponding temperatures in Eq. (3.1),

$$\begin{aligned}\Delta S/Nk_B &= 0.81 \pm 0.04 \quad (\rho^* = 0.4) \\ &= 0.54 \pm 0.05 \quad (\rho^* = 1.0) \,.\end{aligned} \tag{3.4}$$

By contrast, the hard-sphere model has the following entropy of melting[8]:

$$\Delta S/Nk_B = 1.16 \pm 0.10 \,. \tag{3.5}$$

Since the Gaussian core model adopts hard-sphere melting behavior as $\rho \to 0$, its own melting entropy must approach the hard-sphere value in this limit. In that connection, results (3.4) suggest that $\Delta S/Nk_B$ for the Gaussian core model may decline monotonically as density increases. Whether the high density limit for this quantity is positive, or is actually zero, must for the moment remain an open question.

In the low-temperature limit, the body-centered-cubic crystals should behave properly as classical harmonic systems. Remembering that the periodic boundary conditions permit free motion of the center of mass, we expect the mean potential energy to behave thus:

$$\langle \Phi^*(T^*) \rangle = \Phi^*(0) + \tfrac{3}{2}(N-1)T^* + 0(T^{*2}) \,. \tag{3.6}$$

In fact the data presented in Figs. 1 and 2 accurately obey this criterion. However, there is positive curvature unambiguously present in the crystal branches,

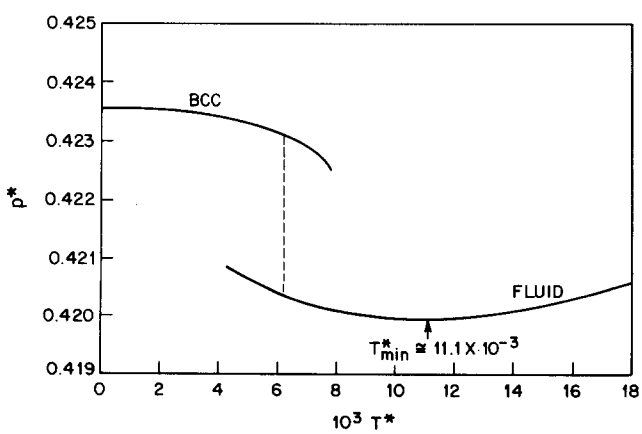


FIG. 3. Reduced pressure $p^*$ at reduced density 0.4.

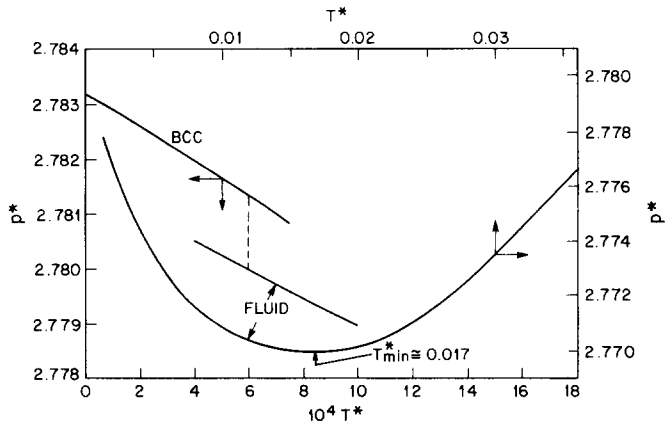


FIG. 4. Reduced pressure $p^*$ at reduced density 1.0.

which we interpret as anharmonic effects in structurally perfect crystals.

In the high-temperature limit, the potential per particle is equal to that for randomly distributed particles:

$$\lim_{T^* \to \infty} \langle \Phi^* \rangle = \tfrac{1}{2}\pi^{3/2}\rho^*(N-1) \tag{3.7}$$

(assuming $l \ll V^{1/3}$). This implies that the fluid branches in Figs. 1 and 2 must turn over and become flat at sufficiently high temperature.

Figures 3 and 4 show the reduced pressures $p^*$ for the two densities 0.4 and 1.0, respectively, where

$$p^* = pl^3/\phi_0 \,. \tag{3.8}$$

The striking feature conveyed in both cases is that pressure declines with increasing temperature, at least up to a point. This region of negative values for $(\partial p/\partial T)_V$ includes the crystal, the transition, and the low-temperature portion of the fluid. In particular, the sudden pressure drop encountered at the transition shows that the melting volume is negative at both densities. We believe it is reasonable to presume that negative melting volumes exist for all $\rho^* \geq 0.4$.

The isothermal variation of entropy $S$ with volume is subject to the following thermodynamic identity:

$$\left(\frac{\partial S}{\partial V}\right)_T = \left(\frac{\partial p}{\partial T}\right)_V \,. \tag{3.9}$$

This implies that compression *increases* entropy (i.e. *decreases* configurational order) in that portion of the $T$, $\rho$ space for which $(\partial p/\partial T)_V$ is negative. Qualitatively speaking, the explaination is that compression tends to convert the spatially inhomogeneous function $\Phi$ to a smoother "mean field" interaction which allows freer particle motion. This is possible primarily because the Gaussian potential is smooth and bounded, with zero slope at the origin.

It is also useful to recall that

$$\left(\frac{\partial V}{\partial p}\right)_T \left(\frac{\partial p}{\partial T}\right)_V \left(\frac{\partial T}{\partial V}\right)_p = -1 \,. \tag{3.10}$$

The first factor on the left (related to isothermal compressibility) is always negative. Consequently,

$$\mathrm{sgn}\left[\left(\frac{\partial p}{\partial T}\right)_V\right] = \mathrm{sgn}\left[\left(\frac{\partial V}{\partial T}\right)_p\right] , \tag{3.11}$$

so that the system exhibits negative thermal expansion (shrinks with increasing $T$ at fixed $p$) whenever $(\partial p/\partial T)_V$ is negative. Heretofore this behavior usually has been associated with substances whose constituent particles engage in tetrahedral bonding; for example, water.[9]

We find that

$$\begin{aligned} p^*/\rho^* T^* &= 170 \pm 8 \quad (\rho^* = 0.4) \\ &= 4600 \pm 400 \quad (\rho^* = 1.0) . \end{aligned} \tag{3.12}$$

These results may be compared with the hard-sphere value at its freezing point[8]:

$$(p/\rho k_B T) = 12.40 \pm 0.20 . \tag{3.13}$$

That the values (3.12) are so much larger is attributable to forced overlap of repelling Gaussian cores at the chosen densities.

It is obvious from the scales in Figs. 3 and 4 that up to and just beyond the respective transition points the pressure changes caused by heating are a small fraction of the total pressure. Thus the coexisting crystal and fluid phases in this density region have isothermal compressibilities both nearly equal to that of the crystal at absolute zero. Having made this observation, we can proceed to estimate the small density changes that would accompany the melting process at constant pressure. We find

$$\begin{aligned} \Delta\rho^*/\rho^* &\cong 3\times 10^{-3} \quad (\rho^* = 0.4) \\ &\cong 2\times 10^{-4} \quad (\rho^* = 1.0) . \end{aligned} \tag{3.14}$$

## IV. LOCAL STRUCTURE

The pair correlation function $g(r)$ provides a useful way to assess the local structure in a classical many-body system. This function is defined by the requirement that the angle-averaged density of particles at distance $r$ from the center of an arbitrarily chosen particle is equal to the overall density $N/V$ times $g(r)$. Exact closed-form expressions incorporating $g(r)$ are available for the thermodynamic energy, pressure,

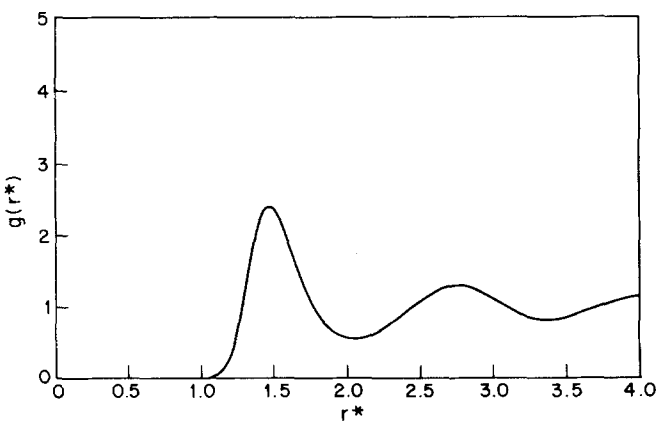


FIG. 5. Fluid phase pair correlation function above the freezing point. $p^* = 0.4$, $T^* = 6.54\times 10^{-3}$.

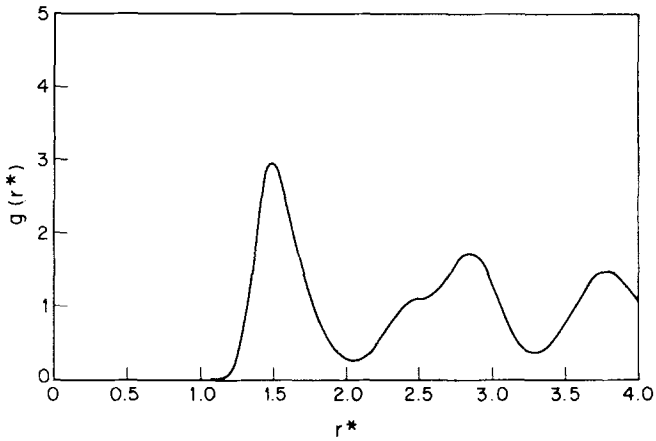


FIG. 6. Pair correlation fucntion for the bcc crystal. $p^* = 0.4$, $T^* = 6.35\times 10^{-3}$. This state is slightly superheated.

and (in the infinite system limit) the isothermal compressibility.[10]

Figure 5 shows $g$ at $T^* = 6.53\times 10^{-3}$, $\rho^* = 0.4$. This is a fluid state just above the freezing point. The shape of this function is qualitatively similar to those that have been determined for other fluids of spherically symmetric particles near their freezing points; for example, argon.[3] Particles tend to collect into concentric coordination shells of decreasing distinctiveness as $r$ increases. Notice that $g$ is essentially zero for $r^* = r/l$ less than about 0.95; for considerably higher temperature ($T^* \gtrsim 0.03$ at $\rho^* = 1$) we have seen frequent particle penetration to zero separation permitted by the fact that the Gaussian interaction is bounded.

Figure 6 presents $g$ for the body-centered-cubic crystal at $T^* = 6.35\times 10^{-3}$, $\rho^* = 0.4$. This crystalline state is slightly superheated, according to Eq. (3.1), but it possesses indefinitely long stability in our computation. It is obvious from Fig. 6 that particle segregation in successive shells is much greater in degree and in range, compared to the fluid. Nevertheless, vibrational motions broaden shells considerably and cause them to overlap. Of course, vibrational broadening can be reduced by lowering the temperature. Figure 7 shows the crystal-phase $g$ at $T^* = 6.76\times 10^{-4}$, still at $\rho^* = 0.4$, where successive shells are much better resolved.

The pair correlation functions obtained at the higher density $\rho^* = 1.0$ are rather similar, provided the distances are scaled by $(\rho^*)^{1/3}$, and temperatures scaled by the corresponding transition temperatures (3.1).

In the bcc crystal at absolute zero, the first and second coordination shells are located at the following distances:

$$\begin{aligned} r_1^* &= 2^{-2/3}\, 3^{1/2} (\rho^*)^{-1/3} \quad (8 \text{ neighbors}) , \\ r_2^* &= 2^{1/3} (\rho^*)^{-1/3} \quad (6 \text{ neighbors}) . \end{aligned} \tag{4.1}$$

Define $a^*$ to be the average of these distances:

$$\begin{aligned} a^* &= (3^{1/2} + 2)\,(32\rho^*)^{-1/3} \\ &\cong 1.1755\,(\rho^*)^{-1/3} . \end{aligned} \tag{4.2}$$

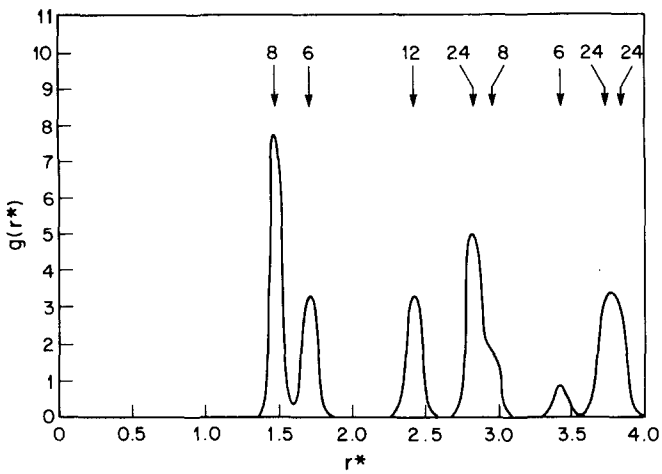


FIG. 7. Pair correlation function in a low-temperature bcc crystal. $p^* = 0.4$, $T^* = 6.76 \times 10^{-4}$. Coordination shells and occupancies for the undistorted lattice are indicated by arrows.

In the perfect crystal at absolute zero, every particle will have exactly eight others within distance $a^*$. But thermal motions will disrupt this neighbor uniformity, either as vibrational motion in the crystal, or by creating packing disorder in the fluid. Therefore it is illuminating to know $P(n, a^*)$, the probability that a randomly selected particle has exactly $n$ neighbors within distance $a^*$.

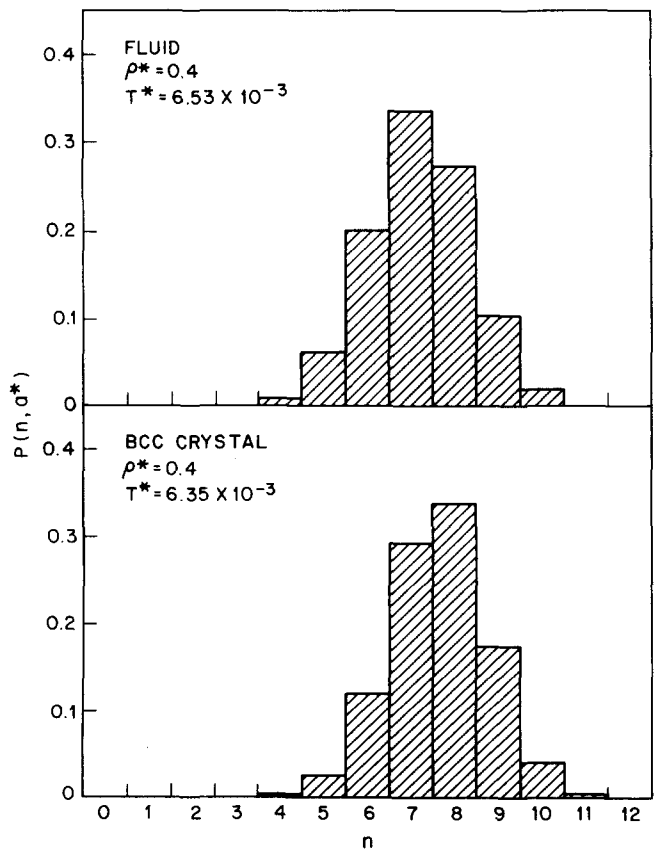


FIG. 8. Comparison of coordination number distributions for fluid and bcc crystal, both at reduced density 0.4.

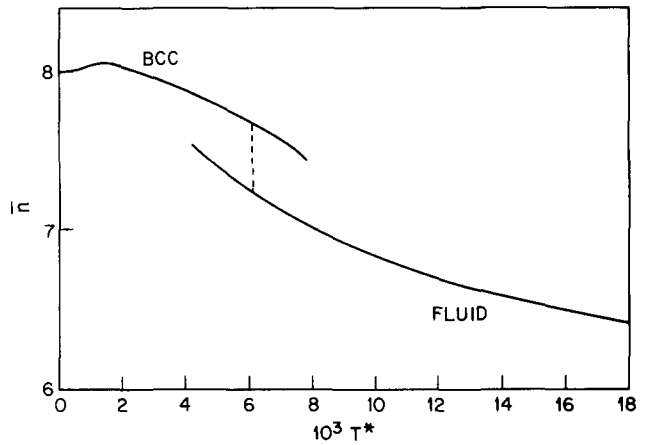


FIG. 9. Average coordination number vs temperature at $p^* = 0.4$.

Figure 8 presents $P(n, a^*)$ in histogram form for two states at $\rho^* = 0.4$. These are the states, one fluid and one crystalline, from which the pair correlation functions in Figs. 5 and 6 were selected. Note that the fluid has a lower average coordination number $\bar{n}$ than does the crystal:

$$\bar{n} = \sum n P(n, a^*) \,. \tag{4.3}$$

The quantity $\bar{n}(T^*)$ is plotted in Fig. 9 for density 0.4. The fact that it increases above eight and passes through a maximum in the low-temperature crystal demonstrates an interesting vibrational phenomenon. The effective radial restoring force for the six second neighbors of any selected particle is less than the same quantity for the eight first neighbors. Consequently a small degree of harmonic thermal motion will cause second neighbors to move inside $a^*$ more frequently than it will cause first neighbors to move outside $a^*$. That $\bar{n}$ begins eventually to decline at sufficiently high temperature in the crystalline phase evidently stems from anharmonicity.

The behavior of $\bar{n}(T^*)$ at the higher density 1.0 is similar to that shown in Fig. 9, except that the temperature scale shifts in accord with the lower transition temperature.

It is very easy to produce amorphous glassy structures by rapidly quenching a fluid state to very low temperature. The quenching is accomplished by setting particle momenta equal to zero, running the system for a few ($\cong 100$) time steps, setting momenta again to zero, etc. By this means the system eventually settles into a local minimum in the $\Phi$ hypersurface. The overwhelming majority of the vast number of $\Phi$ minima for $N = 432$ are amorphous; the chance of producing an ordered crystal this way is negligibly small.

The result of one such quenching at $\rho^* = 1.0$ produced a pair correlation function shown in Fig. 10. Although this state still possesses a positive temperature ($T^* = 7.98 \times 10^{-6}$), the particles are essentially all locked in place, and no perceptible diffusion occurs. For this amorphous structure we find

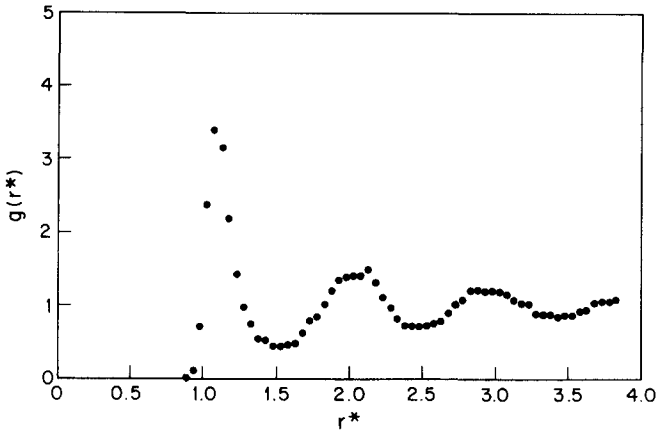


FIG. 10. Amorphous packing pair correlation function. $p^* = 1.0$, $T^* = 7.98 \times 10^{-6}$. The nearly stationary particles have pair distances accumulated in bins of size $\Delta r^* = 0.05$.

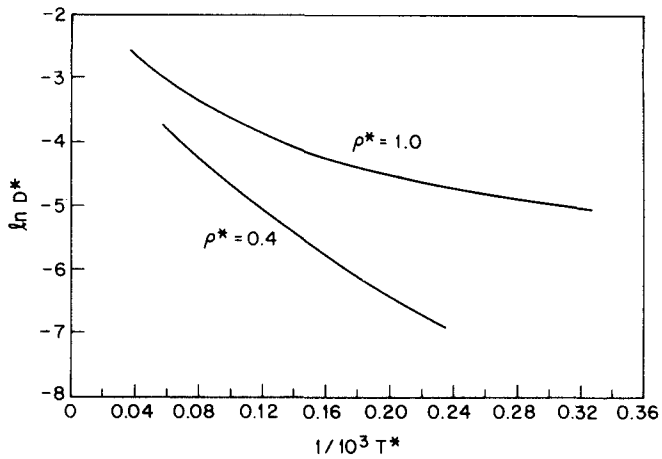


FIG. 12. Temperature variation of the self-diffusion constant.

$$\langle \Phi^* \rangle / N = 2.2845508\ ,$$
$$p^* = 2.7819862\ , \qquad (4.4)$$
$$\bar{n} = 8.0867\ ,$$

which are values roughly in agreement with smooth extrapolations of fluid branch curves for those quantities. Figure 11 exhibits the distribution $P(n, a^*)$ for this amorphous packing, which evidently contains a wide variety of local coordination geometries. Although close-packed particle arrangements may be present [they would be included in $P(12, a^*)$], they are not predominant. The perfect bcc crystal at this temperature would have $P(n, a^*)$ entirely concentrated at $n = 8$.

## V. SELF-DIFFUSION

By monitoring particle displacements as a function of time during the course of the molecular dynamics runs it is possible to calculate the self-diffusion constant, $D^*$. In particular, we have

$$D^* = \lim_{t^* \to \infty} \langle [\mathbf{r}_i^*(t) - \mathbf{r}_i^*(0)]^2 \rangle / 6t^* \ . \qquad (5.1)$$

In the perfect crystal (and also low-temperature amorphous packings) $D^*$ is zero; the mean-square particle deviation approaches an asymptotic limit with time that is related to vibrational amplitudes. However, in the fluid the mean-square deviation rather quickly approaches linear behavior from whose slope we have inferred $D^*$.

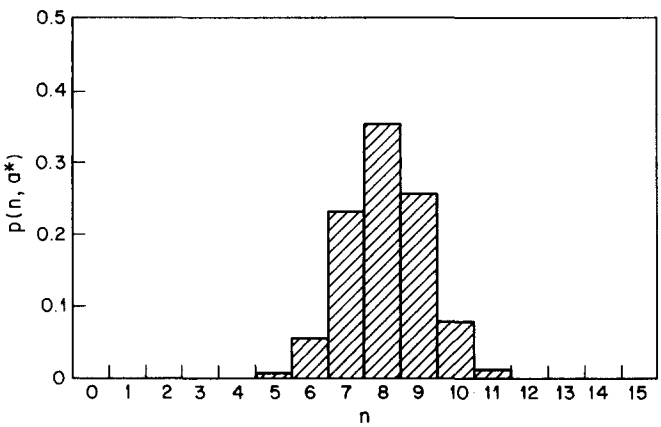


FIG. 11. Coordination number distribution for the amorphous packing of Fig. 10. $p^* = 1.0$, $T^* = 7.98 \times 10^{-6}$, $a^* = 1.1755$.

Our numerical results for $D^*$ at both densities appear in Fig. 12, where $\ln D^*$ is plotted against $1/T^*$. In this form of presentation the slope of the curve is conventionally interpreted in terms of an energy of activation for the diffusion process.[11] The energy of activation obviously decreases as $\rho^*$ increases from 0.4 to 1.0.

The most notable conclusion from our numerical study of $D^*$ is that compressing the fluid isothermally from $\rho^* = 0.4$ to $\rho^* = 1.0$ increases the rate of self-diffusion. At $T^* = 5 \times 10^{-3}$, for instance, $D^*$ increases by about a factor of 7. Of course we have not determined $D^*$ at densities between these extremes, but it seems plausible that $D^*$ is a monotonic function of $\rho^*$, at least for $T^* \leq 10^{-2}$, $\rho^* \geq 0.4$.

The tendency for $D^*$ to increase with $\rho^*$ is analogous to the same observation for water,[5] though the effect is far more dramatic in the Gaussian core model. It indicates a negative volume of activation for self-diffusion; that is, particle displacements are correlated with local contractions. As we have noticed before, contraction (compression) leads to greater particle freedom. From this point of view the negative activation volume for $D^*$ is logically connected to the negative temperature coefficient of pressure [Eq. (3.8)] noted earlier.

## VI. PHASE TRANSFORMATION DYNAMICS

As the perfect crystal is heated slowly from absolute zero, vibrational motions become increasingly anharmonic as their amplitudes increase. This seems to have the effect of locally "softening" the crystal, which is eventually able to shake itself apart into the disordered fluid. We have found that in order for this spontaneous melting of a structurally perfect (defect-free) crystal to occur in a reasonable amount of time (within $10^4\ \Delta t^*$), the reduced temperature must be at least $8 \times 10^{-3}$ at $\rho^* = 0.4$, and at least $7.8 \times 10^{-4}$ at $\rho^* = 1.0$.

We had anticipated at the outset that these instability points would have to be interpreted as upper bounds on the true melting temperatures $T_m^*(\rho^*)$.

But whereas a heated crystal will always melt eventually, a cooled fluid need not crystallize. We have already noted that amorphous glassy structures can be formed by rapid quenching from a stable fluid state. Nevertheless, with sufficient patience in the molecular dynamics study, spontaneous crystallization will initiate if the temperature conditions are appropriate. At $\rho^* = 0.4$ we have never observed freezing unless the fluid was cooled below $T^* = 4.3\times10^{-3}$; at $\rho^* = 1.0$ it was correspondingly necessary to cool the fluid below $T^* = 4.1 \times10^{-4}$.

On account of the constant-energy condition under which the molecular dynamics is carried out, the melting of a crystal is accompanied by an obvious temperature reduction as the latent heat is absorbed. Thus a $\rho^* = 0.4$ perfect crystal which starts melting at $T^* = 8.0 \times10^{-3}$ finally ends up as fluid at $T^* = 6.6\times10^{-3}$. Inversely, the adiabatic freezing of supercooled fluid originally at $\rho^* = 0.4$, $T^* = 4.3\times10^{-3}$ would produce a perfect crystal at $T^* = 5.7\times10^{-3}$. A long sequence of molecular dynamics runs with successive heating and cooling to produce cycling through melting and freezing transitions will trace out hysteresis loops in, for example, the pressure plots as shown in Figs. 3 and 4.

With respect to freezing of the fluid, it is clear that an optimal degree of supercooling exists at which the rate of nucleation is at a maximum. We find, for example, that $\rho^* = 0.4$ flud begins to crystallize about 5 times faster on the average at $T^* = 3.9\times10^{-3}$ than at $T^* = 4.3\times10^{-3}$. However, strong and rapid supercooling of the same fluid to below $T^* = 2.5\times10^{-3}$ slows the rate of diffusion (and hence structural change) so much that freezing becomes unobservably infrequent.

We believe that the thermodynamic transition temperatures can reliably be estimated by the average of the *final* temperatures at which spontaneously frozen and spontaneously melted systems come to rest. This is the basis on which the values stated earlier in Eq. (3.1) were chosen.

While the initiation of spontaneous freezing within the appropriate temperature range appears to be predictable and statistically reproducible, the resulting solid structure is not. Evidently the degree of perfection of the "crystalline" phase is highly variable. We presume that this variability is associated with the crystallographic orientation of the nucleus at which the solid begins to grow. Only rarely will this random orientation closely approximate that possessed by the perfect arrangement of 432 particles in the periodic unit cell. In that unlikely event, the growing crystal would eventually encounter its own image, and the two would grow together without mismatch. Indeed, we seem to have observed one freezing event at $\rho^* = 0.4$ of this ideal kind.

More commonly, the growing crystallite is misaligned with respect to the periodicity cell. The final defective structure then at least contains grain boundaries. These grain boundaries are necessarily regions of remanent particle disorder, and their presence presumably generates strain throughout the crystalline regions. The existence of this mismatch, disorder, and strain are obvious from all the quantities by which the phase transitions are monitored. In effect, one observes that the transition fails to go to completion. Average potential and pressure in this type of circumstance typically shift only by 60%–80% of the full changes expected if a defect-free crystal were to form. Similar interpolated values for $g(r)$ and $P(n, a^*)$ are also obtained.

Although the unreproducibly defective nature of the frozen material is disadvantageous for study of equilibrium crystal properties, it nevertheless provides an opportunity. The disordered grain-boundary region can act as an effective nucleation site for melting, and thus give a better upper bound on $T_m^*$ than was provided by the perfect crystal melting. The defective solid samples also help to fix $T_f^*$ as well. Upon slowly warming such a sample, we first find that annealing takes place as some disorder freezes out. This presumably occurs below the thermodynamic $T_f^*$. Further heating eventually causes both $T_f^*$ and $T_m^*$ to be exceeded, at which point we see remelting of the still somewhat defective solid take place. These careful observations of annealing and remelting constitute an independent means for fixing the thermodynamic transition and have been used to confirm the validity of Eq. (3.1).

A fluid-phase analog of the defective solid can also be produced. To do this, a perfect crystal (originally constructed at absolute zero and warmed) is taken to the temperature at which it shakes apart into fluid. But just before the melting goes to completion the molecular dynamics process is interrupted. At that stage the system is mostly fluid, but contains an unmelted crystal fragment which potentially can act as a "seed" for freezing. If the momenta are then scaled downward to bring the temperature below $T_f^*$, crystallization quickly ensues. In fact, there is high probability that the seed will be properly aligned to yield a defect-free crystal, since it was produced itself from such a structure. We have also used this seed technique to confirm the transition temperature assignment at $\rho^* = 1.0$.

## VII. DISCUSSION

Several aspects of the Gaussian core model that have not yet been studied deserve future attention by the molecular dynamics method. One of these is location of the density at which $T_m(\rho^*)$ and $T_f(\rho^*)$ attain their common maximum. Another would be the study of the transition entropy at densities above $\rho^* = 1.0$ to see if this quantity becomes arbitrarily small in the high density limit. It would also be interesting to study vacancy and interstitial diffusion in the crystal by varying $N$ slightly away from 432.

The analogy between anomalous thermodynamic properties in the present model and in water can be examined further. The shear viscosity of liquid water is known to decrease with increasing pressure, below 30 °C[12]; furthermore, this liquid's isothermal compressibility has a negative temperature derivative below

46 °C.[13] These phenomena both are contrary to the behavior of normal liquids. It would be illuminating to establish whether or not these anomalies also exist in the Gaussian core model.

Now that molecular dynamics simulation has begun to create a data base for the Gaussian core model, it is appropriate to develop theoretical methods for predicting and understanding its properties. The abnormalities of the fluid phase might be amenable to study through standard $g(r)$ integral equation methods,[14] though it is possible that the approximations used in deducing these integral equations might suppress those abnormalities.

We have already mentioned the opportunity for deriving an extended set of exact coefficients for the inverse temperature series expansion of the partition function. In the infinite-system size limit such a series must have a vanishing radius of convergence and would require special summation techniques for analysis. On the other hand, it may be more useful to employ this series for finite $N$ and $V$, where in fact it does have a nonzero convergence radius. In this case the series may permit study of location of partition function zeros in the complex temperature plane. The convergence of these zeros onto the real axis as $N$ and $V$ become large would locate $T_m$ and $T_f$, and would show how the transition sharpens as the number of degrees of freedom in the system increases.

[1] F. H. Stillinger, J. Chem. Phys. 65, 3968 (1976).
[2] H. Cramer, *Mathematical Methods of Statistics*, (Princeton U. P. Princeton, NJ, 1946), Chap. 15.
[3] A. Rahman, Phys. Rev. Sect. A 136, 405 (1964).
[4] D. Eisenberg and W. Kauzmann, *The Structure and Properties of Water* (Oxford U. P., New York, 1969), p. 183.
[5] D. J. Wilbur, T. DeFries, and J. Jonas, J. Chem. Phys. 65, 1783 (1976).
[6] F. H. Stillinger, Philos. Trans. R. Soc. London B 278, 97 (1977).
[7] C. W. Gear, "The Numerical Integration of Ordinary Differential Equations of Various Orders," Argonne National Lab. Rep. ANL-7126 January, 1966.
[8] W. G. Hoover and F. H. Ree, J. Chem. Phys. 49, 3609 (1968).
[9] C. A. Angell and H. Kanno, Science 193, 1121 (1976).
[10] T. L. Hill, *Statistical Mechanics* (McGraw-Hill, New York, 1956), Chap. 6.
[11] S. Glasstone, K. J. Laidler, and H. Eyring, *The Theory of Rate Processes* (McGraw-Hill, New York, 1941), pp. 522–528.
[12] Reference 4, p. 222.
[13] Reference 4, p. 185.
[14] S. A. Rice and P. Gray, *The Statistical Mechanics of Simple Liquids* (Wiley Interscience, New York, 1965), Chap. 2.

# Erratum: Study of melting and freezing in the Gaussian core model by molecular dynamics simulation [J. Chem. Phys. 68, 3837 (1978)]

Frank H. Stillinger and Thomas A. Weber

*Bell Laboratories, Murray Hill, New Jersey 07974*

The text of this erratum was interchanged with that of the preceding erratum on page 4322 in the 1 November 1978 issue of the Journal of Chemical Physics.

Owing to errors in typesetting, the captions to Figs. 5, 6, 7, 9, 10, and 11 require correction. For each of these, replace the symbol $p^*$ by the reduced density symbol $\rho^*$.

 0021-9606/79/021074-01$00.00 